Supporting Information

Sodium ions pre-intercalation Regulate Electron Density and Structural Stability of Vanadium Oxide Nanowire for Ca-Ion Battery

Huajie Feng, [a] Yize Wang, [a] Wenda Qiu,*[b] Zixi Liu, [a] Yaping Tao [d] and Xihong Lu [c]

[a] *Key Laboratory of Electrochemical Energy Storage and Energy Conversion of Hainan Province, Hainan Normal University, Haikou 571158, Hainan, China*

[b] *Guangdong Industry Polytechnic College, Guangzhou 510300, Guangdong, China*

[c] *MOE of the Key Laboratory of Bioinorganic and Synthetic Chemistry, KLGHEI of Environment and Energy Chemistry, School of Chemistry, Sun Yat-Sen University, Guangzhou 510275, Guangdong, China*

[d] *College of Physics and Electronic Information & Henan Key Laboratory of Electromagnetic Transformation and Detection, Luoyang Normal University, Luoyang 471934, China*

***Corresponding Author.**

E-mail: qiuwd3@mail3.sysu.edu.cn (W.D. Qiu)

Calculations:

Specific capacities ($C_{cell\text{-}s}$) of the cell were estimated from the discharge curve using the following equations:

$$C_{cell-s} = \frac{\int_0^{\Delta t} I \times dt}{m} \quad (2)$$

where $C_{cell\text{-}s}$ (mA h g^{-1}) is the specific capacity of the CIB, I (mA) is the applied discharging current, Δt (h) is the discharging time and m (g) is the mass of the active material.

The chemical diffusion coefficient of Ca^{2+} can be calculated based on the following equation:

$$D_{GITT} = \frac{4}{\pi\tau}\left(\frac{n_m V_m}{S}\right)^2 \left(\frac{\Delta E_s}{\Delta E_t}\right)^2 \quad (5)$$

Here, τ (s) is the duration of the current pulse; n_m (mol) is the number of moles; V_m (cm^3 mol^{-1}) is the molar volume of the electrode; S (cm^2) is the electrode/electrolyte contact area; ΔE_s is the steady state voltage change due to the current pulse, and ΔE_t is the voltage change during the constant current pulse, eliminating the *iR* drop.

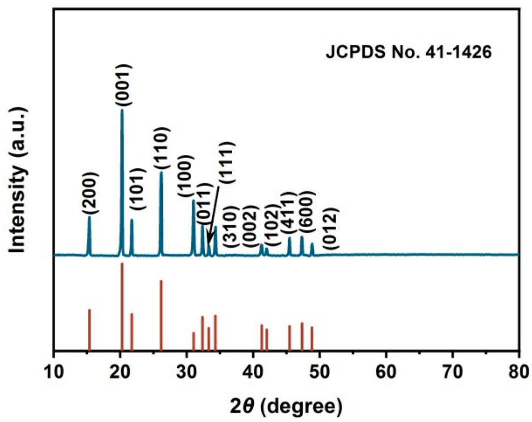

Figure S1. XRD pattern of V_2O_5 NW.

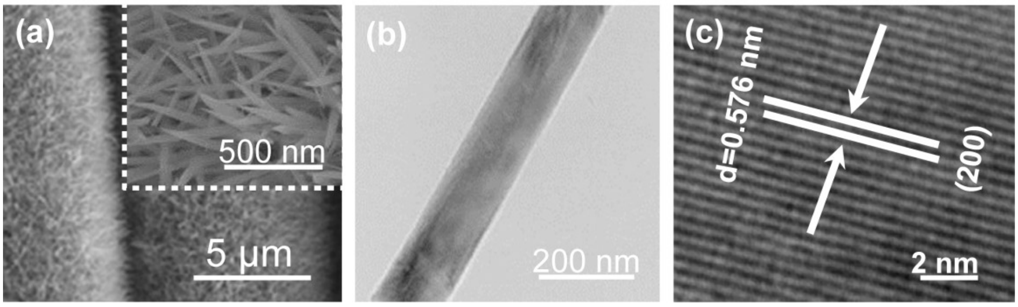

Figure S2. (a) SEM, (b) TEM, and (c) HRTEM images of V_2O_5 NW.

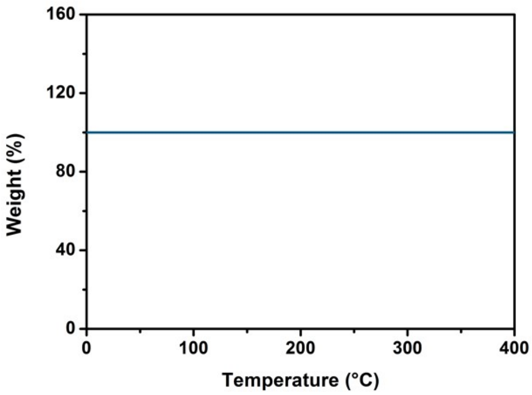

Figure S3. TGA curves of NVO NW at a heating rate of 5 °C min^{-1} under N_2 flowing atmosphere.

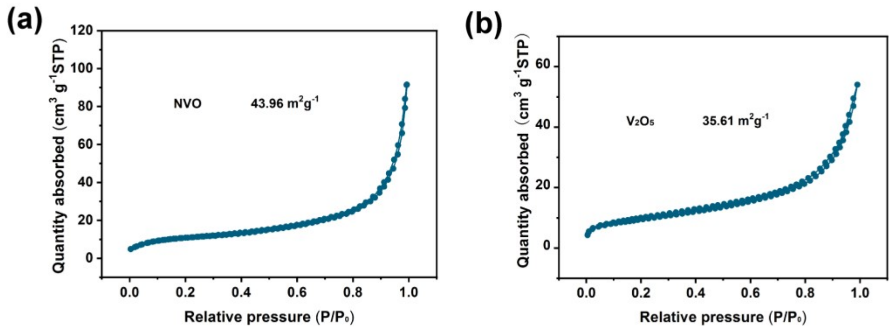

Figure S4. N_2 adsorption-desorption isotherm of (a) NVO and (b) V_2O_5 NW.

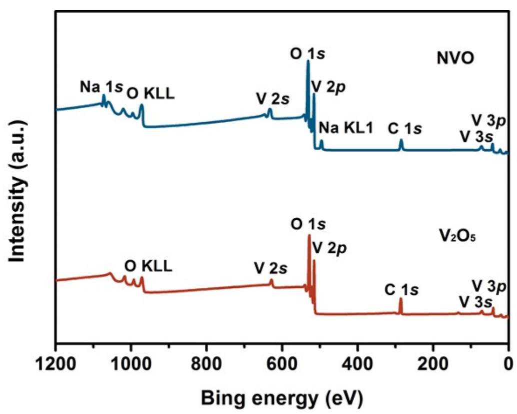

Figure S5. Survey spectra of V_2O_5 and NVO NW.

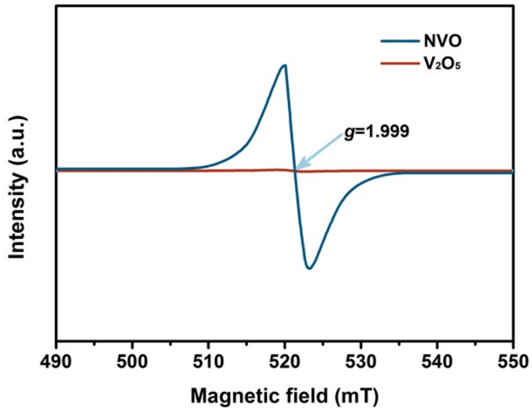

Figure S6. EPR spectra of NVO and V_2O_5 NW.

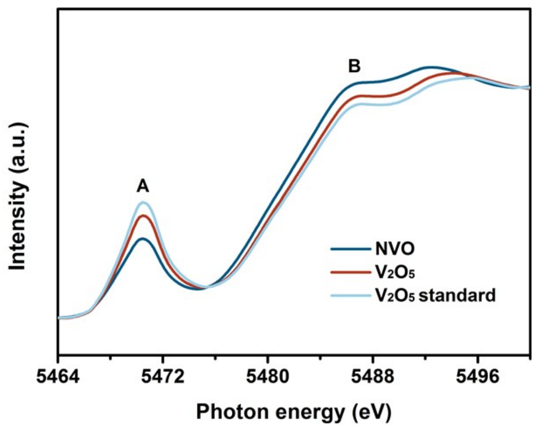

Figure S7. V K-edge spectra of NVO and V_2O_5 NW.

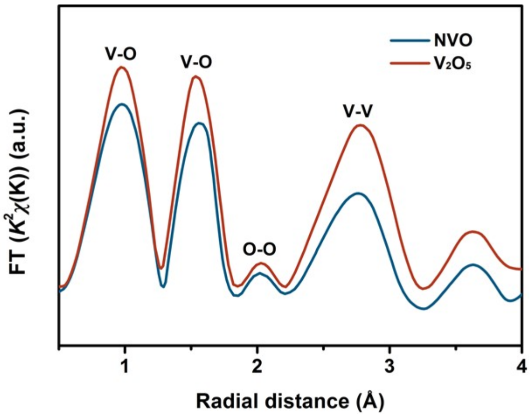

Figure S8. Fourier transforms of V K-edge EXAFS (k^3-weighted) for NVO and V_2O_5 NW.

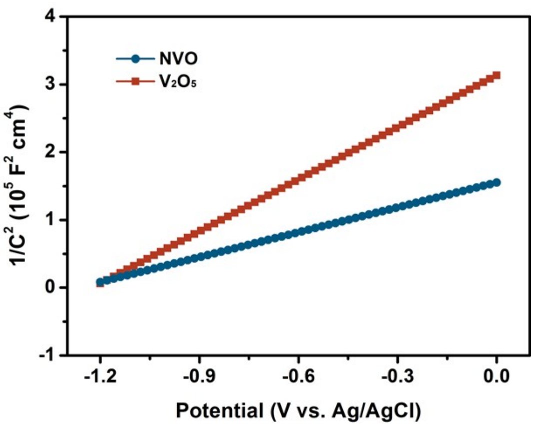

Figure S9. Mott−Schottky plots of NVO and V_2O_5 NW.

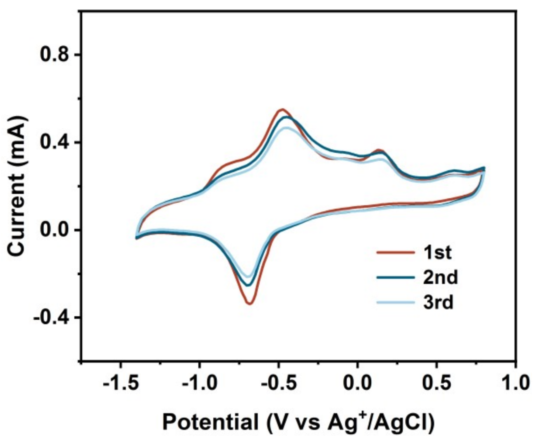

Figure S10. CV curves of V_2O_5 NW electrode at o.5 mV s^{-1}.

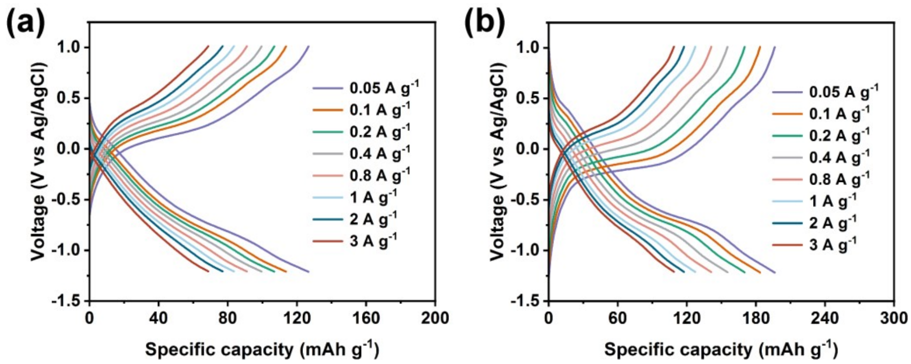

Figure S11. Galvanostatic charge–discharge profiles at different current densities of

(a) V_2O_5 and (b) NVO NW electrodes.

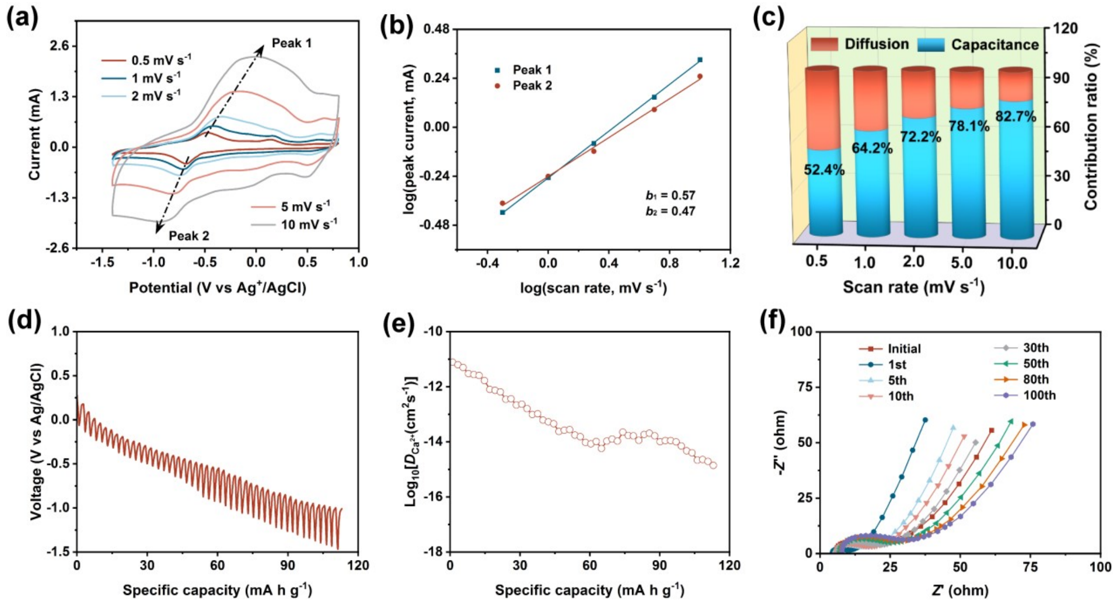

Figure S12. Reaction kinetic of V_2O_5 electrode: (a) CV curves of different scan rates, (b) Log(i) versus log(v) plots, (c) capacitive contribution under various scan rates, (d) discharge GITT curves at 0.1 A g^{-1}, (e) the calculated $D_{Ca^{2+}}$, and (f) Nyquist plots after different cycles.

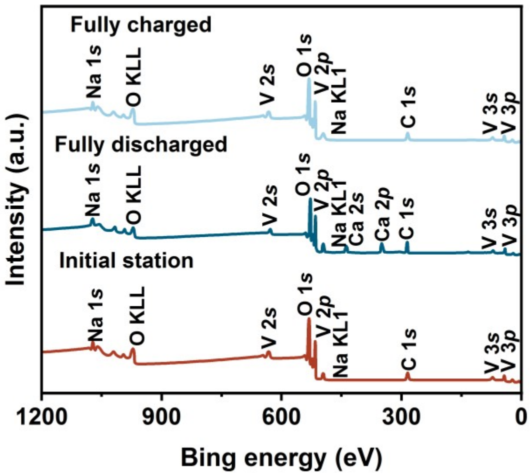

Figure S13. Survey spectra of NVO NW electrode at the initial, fully discharged, and fully charged station.

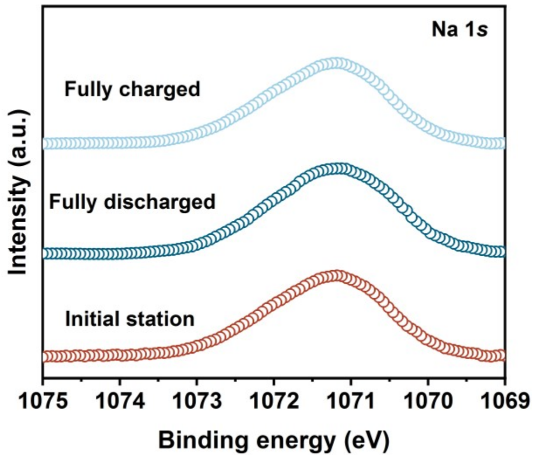

Figure S14. Na 1*s* spectra of NVO NW electrode at the initial, fully discharged, and fully charged station.

Table S1. The ICP-OES result of the NVO electrode at different cycles.

Sample	Elements	Concentration (mg L^{-1})	Molar ratio (Na : Ca : V)
	Na	1.6807	
Initial state	Ca	0.0067	0.351 : 0.0008 : 2
	V	21.28	
	Na	1.6886	
After 1st	Ca	0.3305	0.321 : 0.036 : 2
	V	23.3844	
	Na	1.6491	
After 5th	Ca	0.2154	0.373 : 0.028 : 2
	V	19.5924	
	Na	1.6253	
After 10th	Ca	0.2578	0.341 : 0.031 : 2
	V	21.1838	
	Na	1.6748	
After 20th	Ca	0.2801	0.364 : 0.035 : 2
	V	20.3897	
	Na	1.6609	
After 50th	Ca	0.2714	0.362 : 0.034 : 2
	V	20.3322	
	Na	1.6576	
After 80th	Ca	0.2573	0.325 : 0.029 : 2
	V	20.602	
	Na	1.6788	
After 100th	Ca	0.2852	0.338 : 0.033 : 2
	V	22.0106	

Table S2. Electrochemical performance comparison with reported cathode materials for CIBs.

Cathodes	Capacity (Max) (mA h g^{-1})	Rate capacity (mA h g^{-1})	Capacity retention/Cycle number/Current density (A g^{-1})	Ref.
NVO NW	196.3 (0.05 A g^{-1})	196.3 (0.05 A g^{-1}) 108.8 (3.9 A g^{-1})	93.1%/2000/2.0	This work
CaV_6O_{16}•$2.8H_2O$	175.2 (0.05 A g^{-1})	175.2 (0.05 A g^{-1}) 69 (0.5 A g^{-1})	93%/1000/0.5	1
$K_{0.5}V_2O_5$	100 (0.013 A g^{-1})	100 (0.013 A g^{-1}) 50 (0.13 A g^{-1})	92%/100/0.067	2
$Na_{1.5}VPO_{4.8}F_{0.7}$	87 (0.01 A g^{-1})	87 (0.01 A g^{-1}) 43.8 (0.5 A g^{-1})	90%/500/0.05	3
$KFeFe(CN)_6$	67 (0.17 A g^{-1})	67 (0.17 A g^{-1}) 55 (3.4 A g^{-1})	88.6%/5000/0.85	4
$Mg_{0.25}V_2O_5$•H_2O	122 (0.02 A g^{-1})	122 (0.02 A g^{-1}) 70 (0.1 A g^{-1})	87.1%/500/0.1	5
$Ca_{0.4}MnO_2$	86 (0.1675 A g^{-1})	86 (0.1675 A g^{-1}) 35 (1.675 A g^{-1})	83%/150/0.66	6
Na_2FePO_4F	120 (0.023 A g^{-1})	120 (0.023 A g^{-1}) 68 (0.072 A g^{-1})	83%/80/0.125	7

Ca_xCuHCF	58 (0.004 A g^{-1})	58 (0.004 A g^{-1}) 37.8 (0.8 A g^{-1})	80%/4000/0.2	8
$Ca_{0.28}V_2O_5$•H_2O	136 (0.01 A g^{-1})	136 (0.01 A g^{-1}) 101 (0.05 A g^{-1})	74%/50/0.03	9
$Ca_{0.13}MoO_3\cdot(H_2O)_{0.41}$	192 (0.086 A g^{-1})	192 (0.086 A g^{-1}) 109 (0.3426 A g^{-1})	72.8%/50/0.3426	10
$K_2V_6O_{16}$	113.9 (0.02 A g^{-1})	113.9 (0.02 A g^{-1}) 60 (0.1 A g^{-1})	66.5%/200/0.1	11
$VOPO_4$•$2H_2O$	117.7 (0.01 A g^{-1})	117.7 (0.01 A g^{-1}) 42.6 (0.2 A g^{-1})	65%/200/0.1	12
β-$Ag_{0.33}V_2O_5$	179 (0.012 A g^{-1})	179 (0.012 A g^{-1}) 28.6 (0.12 A g^{-1})	47%/50/0.12	13

Table S3. Comparasion of the $D_{Ca^{2+}}$ with some reported electrode materials.

Electrode Materials	$D_{Ca^{2+}}$ (cm^2s^{-1})	Ref.
NVO NW	$10^{-11} \sim 10^{-12}$	This work
TiO_2/WO_xH_y	$10^{-11} \sim 10^{-13}$	14
α-MoO_3	$10^{-11} \sim 10^{-13}$	15
MnVO	10^{-12}	16
Nano-Si	$10^{-12} \sim 10^{-13}$	17
$Li_xAg_{0.5}V_2O_5$	$10^{-12} \sim 10^{-14}$	18
MnO_2 nanospheres	$10^{-12} \sim 10^{-15}$	19
δ-MnO_2	$10^{-12} \sim 10^{-15}$	20
Graphene Scroll Coated α-MnO_2	$10^{-12} \sim 10^{-17}$	21
VOG	10^{-13}	22
α-MnO_2	$10^{-15} \sim 10^{-17}$	23
TiO_2	$10^{-15} \sim 10^{-17}$	24
$LiFePO_4$	$10^{-15} \sim 10^{-19}$	25

Table S4. The EIS data of NVO NW electrode after different cycles.

NVO	R_s (Ω)	R_{ct} (Ω)
Initial	1.74	8.46
1st	1.37	3.14
5th	1.67	5.63
10th	1.57	6.47
30th	1.68	9.05
50th	1.56	7.77
80th	1.91	6.30
100th	1.98	7.31

Table S5. The EIS data of V_2O_5 NW electrode after different cycles.

V_2O_5	R_s (Ω)	R_{ct} (Ω)
Initial	5.56	15.04
1st	4.38	5.58
5th	5.34	10.01
10th	5.85	11.50
30th	6.37	14.08
50th	6.91	17.81
80th	7.33	20.20

100th	7.68	21.85

References

1. J. Wang, J. Wang, Y. Jiang, F. Xiong, S. Tan, F. Qiao, J. Chen, Q. An and L. Mai, CaV_6O_{16}•$2.8H_2O$ with Ca^{2+} Pillar and Water Lubrication as a High-Rate and Long-Life Cathode Material for Ca-Ion Batteries, *Adv. Funct. Mater.*, 2022, **32**, 2113030.

2. M. E. Purbarani, J. Hyoung and S.T. Hong, Crystal-water-free potassium vanadium bronze ($K_{0.5}V_2O_5$) as a cathode material for Ca-ion batteries, *ACS Appl. Energy Mater.*, 2021, **4**, 7487-7491.

3. Z.L. Xu, J. Park, J. Wang, H. Moon, G. Yoon, J. Lim, Y.J. Ko, S.P. Cho, S.Y. Lee and K. Kang, A new high-voltage calcium intercalation host for ultra-stable and high-power calcium rechargeable batteries, *Nat. commun.*, 2021, **12**, 3369.

4. C. Lee and S.-K. Jeong, Modulating the hydration number of calcium ions by varying the electrolyte concentration: Electrochemical performance in a Prussian blue electrode/aqueous electrolyte system for calcium-ion batteries, *Electrochim. Acta*, 2018, **265**, 430-436.

5. X. Xu, M. Duan, Y. Yue, Q. Li, X. Zhang, L. Wu, P. Wu, B. Song and L. Mai, Bilayered $Mg_{0.25}V_2O_5$• H_2O as a stable cathode for rechargeable Ca-ion batteries, *ACS Energy Lett.*, 2019, **4**, 1328-1335.

6. X. Tang, D. Zhou, B. Zhang, S. Wang, P. Li, H. Liu, X. Guo, P. Jaumaux, X. Gao and Y. Fu, A universal strategy towards high–energy aqueous multivalent–ion batteries, *Nat. Commun.*, 2021, **12**, 2857.

7. N. Kuperman, P. Padigi, G. Goncher, D. Evans, J. Thiebes and R. Solanki, High performance Prussian Blue cathode for nonaqueous Ca-ion intercalation battery, *J. Power Sources*, 2017, **342**, 414-418.

8. S. Gheytani, Y. Liang, F. Wu, Y. Jing, H. Dong, K. K. Rao, X. Chi, F. Fang and Y. Yao, An aqueous Ca-ion battery, *Adv. Sci.*, 2017, **4**, 1700465.

9. B. Jeon, H. H. Kwak and S.T. Hong, Bilayered $Ca_{0.28}V_2O_5$• H_2O: High-Capacity Cathode Material for Rechargeable Ca-Ion Batteries and Its Charge Storage Mechanism, *Chem. Mater.*, 2022, **34**, 1491-1498.

10. M. S. Chae, H. H. Kwak and S.-T. Hong, Calcium molybdenum bronze as a stable high-capacity cathode material for calcium-ion batteries, *ACS Appl. Energy Mater.*, 2020, **3**, 5107-5112.

11. L.W. Dong, R.G. Xu, P.P. Wang, S.C. Sun, Y. Li, L. Zhen and C.Y. Xu, Layered potassium vanadate $K_2V_6O_{16}$ nanowires: A stable and high capacity cathode material for calcium-ion batteries, *J. Power Sources*, 2020, **479**, 228793.

12. J. Wang, S. Tan, F. Xiong, R. Yu, P. Wu, L. Cui and Q. An, $VOPO_4$• $2H_2O$ as a new cathode material for rechargeable Ca-ion batteries, *Chem. Commun.*, 2020, **56**, 3805-3808.

13. J. Hyoung, J. W. Heo, B. Jeon and S.-T. Hong, Silver vanadium bronze, β-$Ag_{0.33}V_2O_5$: crystal-water-free high-capacity cathode material for rechargeable Ca-ion batteries, *J. Mater. Chem. A*, 2021, **9**, 20776-20782.

14. T. Facci and F. Huguenin, Spectroelectrochemical properties and lithium ion storage in self-assembled nanocomposites from TiO_2, *Langmuir*, 2010, **26**, 4489-

4496.

15. M. Yu, H. Shao, G. Wang, F. Yang, C. Liang, P. Rozier, C.Z. Wang, X. Lu, P. Simon and X. Feng, Interlayer gap widened α-phase molybdenum trioxide as high-rate anodes for dual-ion-intercalation energy storage devices, *Nat. commun.*, 2020, **11**, 1348.
16. C. Liu, Z. Neale, J. Zheng, X. Jia, J. Huang, M. Yan, M. Tian, M. Wang, J. Yang and G. Cao, Expanded hydrated vanadate for high-performance aqueous zinc-ion batteries, *Energ. Environ. Sci.*, 2019, **12**, 2273-2285.
17. N. Ding, J. Xu, Y. Yao, G. Wegner, X. Fang, C. Chen and I. Lieberwirth, Determination of the diffusion coefficient of lithium ions in nano-Si, *Solid State Ionics*, 2009, **180**, 222-225.
18. F. Huang, Z.W. Fu and Q.Z. Qin, A novel $Li_2Ag_{0.5}V_2O_5$ composite film cathode for all-solid-state lithium batteries, *Electrochem. commun.*, 2003, **5**, 262-266.
19. J. Wang, J.-G. Wang, H. Liu, C. Wei and F. Kang, Zinc ion stabilized MnO_2 nanospheres for high capacity and long lifespan aqueous zinc-ion batteries, *J. Mater. Chem. A*, 2019, **7**, 13727-13735.
20. C. Guo, H. Liu, J. Li, Z. Hou, J. Liang, J. Zhou, Y. Zhu and Y. Qian, Ultrathin δ-MnO_2 nanosheets as cathode for aqueous rechargeable zinc ion battery, *Electrochim. Acta*, 2019, **304**, 370-377.
21. B. Wu, G. Zhang, M. Yan, T. Xiong, P. He, L. He, X. Xu and L. Mai, Graphene scroll-coated α−MnO_2 nanowires as high‐performance cathode materials for aqueous Zn-ion battery, *Small*, 2018, **14**, 1703850.

22. M. Yan, P. He, Y. Chen, S. Wang, Q. Wei, K. Zhao, X. Xu, Q. An, Y. Shuang and Y. Shao, Water‑lubricated intercalation in V_2O_5•$n$$H_2O$ for high-capacity and high-rate aqueous rechargeable zinc batteries, *Adv. Mater.*, 2018, **30**, 1703725.

23. B. Lee, H. R. Lee, H. Kim, K. Y. Chung, B. W. Cho and S. H. Oh, Elucidating the intercalation mechanism of zinc ions into α-MnO_2 for rechargeable zinc batteries, *Chem. commun.*, 2015, **51**, 9265-9268.

24. M.S. Wu, M.J. Wang, J.J. Jow, W.D. Yang, C.Y. Hsieh and H.M. Tsai, Electrochemical fabrication of anatase TiO_2 nanostructure as an anode material for aqueous lithium-ion batteries, *J. Power Sources*, 2008, **185**, 1420-1424.

25. K. Tang, X. Yu, J. Sun, H. Li and X. Huang, Kinetic analysis on $LiFePO_4$ thin films by CV, GITT, and EIS, *Electrochim. Acta*, 2011, **56**, 4869-4875.